Temperature and Stagnation Effects on Ozone Sensitivity to NOx and VOC: An Adjoint Modeling Study in Central California

Yuhan Wang[1], Lucas Bastien[2,3], Yuan Wang[1], Ling Jin[3], and Robert Harley[4]

[1]Department of Earth System Science, Stanford University, Stanford, CA 94305, USA
[2]Institute of Environmental Geosciences, National Centre for Scientific Research, Grenoble 38058, France
[3]Energy Technologies Area, Lawrence Berkeley National Laboratory, Berkeley, CA 94720, USA
[4]Department of Civil and Environmental Engineering, University of California, Berkeley, CA 94720, USA

Correspondence to: Ling Jin (ljin@lbl.gov) and Robert Harley (harley@ce.berkeley.edu)

Abstract. Extreme weather events like heatwaves and stagnation are increasing with climate change. While their effects on ozone levels have been extensively studied, how extreme weather alters O_3-NO_x-VOC sensitivity and optimal mitigation strategies is less explored. Here, we apply the CMAQ adjoint model over central California to quantify ozone sensitivity to spatiotemporally resolved precursor emissions under three meteorological scenarios (baseline, high-T, and stagnation) and three emission years (2000, 2012, and 2022). Results show that meteorology-induced changes in sensitivity are comparable in magnitude to those from decadal emission reductions. Higher temperature (+5 °C) amplifies ozone sensitivity to both NO_x and VOC, with the largest relative increase in biogenic VOC sources. High-T conditions shift ozone chemistry toward NO_x limitation under a VOC-limited emission scenario, but increase the relative importance of VOC control for a NO_x-limited scenario. Stagnation consistently pushes ozone chemistry toward VOC limitation across emission scenarios, increasing VOC sensitivity by a factor of ~3-4. Stagnation also spatially shifts influential source areas, especially for NO_x, and temporally amplifies prior-day emission impacts due to enhanced pollutant carryover. As the study domain transitions to a NO_x-limited regime over time, we identify a growing subset of "climate-resilient" source targets that remain impactful across meteorological scenarios, along with spatial convergence in optimal locations for NO_x and VOC emission control. These findings underscore both the need and feasibility to consider meteorological extremes in the design of ozone mitigation strategies for a warming climate.

1 Introduction

Heatwaves and atmospheric stagnation events are increasing in frequency, intensity and duration due to climate change (Meehl and Tebaldi, 2004; Horton et al., 2014; Hou and Wu, 2016). Between 1951-1980 and 1981-2010, the occurrence of heatwaves and stagnation events increased by 25.8±3.3% and 4.5±0.8%, respectively, for non-polar continental regions (Hou and Wu, 2016). Meteorological conditions modulate air pollution by changing weather-dependent emissions (e.g., from biogenic sources), by regulating the transport and removal of emitted pollutants, and by altering temperature- and light-sensitive chemical reaction rates. Although extremely high temperature may suppress ozone (O_3) formation (Steiner et al., 2010), most evidence robustly link heatwaves and stagnation events to elevated ozone pollution (Gao et al., 2013; Hou and Wu, 2016; Shen et al., 2016; Schnell and Prather, 2017; Zhang et al., 2018). Given ozone's adverse impacts on human health and ecosystems (Jerrett et al., 2009; Krupa et al., 2001), effective ozone mitigation under these pollution-favoring conditions is critical.

While many studies have examined meteorological control on ozone levels, far fewer have addressed how these meteorological conditions alter ozone sensitivity to precursor emissions and subsequently change effectiveness of emission control programs. While the former is important for identifying challenges, the latter is crucial for shaping solutions.

Ground-level ozone forms through photochemical reactions involving its precursors: nitrogen oxides (NO_x) and volatile organic compounds (VOC). This O_3-NO_x-VOC chemistry is complex and highly nonlinear (Pusede et al., 2015; Kleinman, 2005). In environments with high VOC/NO_x ratios (*NO_x-limited regime*), ozone formation is primarily controlled by NO_x availability and relatively insensitive to VOC changes. Conversely, when the VOC/NO_x ratio is low (*VOC-limited regime*), controlling VOC is

40 more effective; NO_x reductions may increase HO_x radicals and decrease ozone titration in this regime, thereby exacerbating ozone pollution. A *transition regime* exists between NO_x- and VOC-limited conditions. Across these regimes, ozone responses to precursor reductions can vary greatly in magnitude and sign, depending on where, when, and which precursor emissions are reduced. Knowledge about O_3-NO_x-VOC sensitivities is therefore key to identifying and controlling emissions from the most influential sources.

45 Some studies have explored how warming shifts ozone sensitivities and their conclusions vary. Baertsch-Ritter et al. (2004) perturbed temperature by up to +10 °C in a 3D air quality model for northern Italy, finding that VOC-limited areas expand with higher temperature, primarily because it promotes peroxyacetyl nitrate (PAN) decomposition and increases NO_x availability. Similarly, Jin et al. (2010) found increased sensitivity to VOC and decreased sensitivity to NO_x under a +2 °C temperature perturbation for the San Francisco Bay area. They attributed these sensitivity changes to elevated radical generation, which

50 amplifies VOC oxidation and accelerates NO_x removal. In contrast, some observational studies have inferred that ozone chemistry becomes more NO_x-limited at high temperatures. Yang et al. (2021) and Huang et al. (2025) analyzed measurements in Shanghai and the Pearl River Delta in China, and diagnosed an ozone regime switch from primarily VOC-limited to transitional or NO_x-limited when exceeding a region-specific temperature threshold. Studies in California's San Joaquin Valley and Los Angeles air basins found strong temperature dependencies for some VOC sources, such as evaporative and biogenic processes

55 (Pusede and Cohen, 2012; Pusede et al., 2014; Nussbaumer and Cohen, 2020; Pfannerstill et al., 2024). They pointed out that VOC reactivity rises with temperature, whereas NO_x reactivity is relatively temperature-invariant. On hotter days, observed increases in weekend O_3 relative to weekdays tend to be attenuated (this suggests a shift to a more NO_x-limited regime), though some sites and years show opposite trends (increasingly VOC-limited conditions). These contrasting findings likely arise from differences in baseline chemical regimes, VOC source profiles, and the temperature ranges examined.

60 Even fewer studies have quantified the effects of stagnation events on ozone sensitivity. Prior modeling evidence generally suggests that ozone formation regimes tend to become more VOC-limited when wind speeds, boundary layer heights, and humidity are low – all are characteristic features of stagnation events (Biswas and Rao, 2001; Baertsch-Ritter et al., 2004; Jin et al., 2008, 2010, 2013). Biswas and Rao (2001) argued that in well-ventilated environments, NO_x is removed more rapidly than VOC as air masses age photochemically, leading to a shift toward NO_x-limited conditions. In contrast, weak dilution (slow wind

65 speeds and shallow boundary layer heights) limit NO_x removal and maintain more VOC-limited conditions. Baertsch-Ritter et al. (2004) also report a slight expansion of VOC-limited areas under low-humidity conditions, though the water vapor influence is expected to be weak overall. Jin et al. (2013) simulated a stagnation event in California's San Joaquin Valley, incorporating changes in all meteorological variables and biogenic emissions. Using perturbation-based sensitivity analysis, they showed that stagnation enhances the relative importance of VOC control and reduces the influence of upwind sources. As stagnation affects

70 both transport patterns and chemical regimes, the most relevant sources for effective ozone mitigation are also expected to shift, but systematic investigations of such impacts are lacking.

Most of the prior studies use either observations or model perturbations to derive ozone sensitivity and formation regime. Observation-based diagnostics include ground-based indicators like ozone production efficiency ($\Delta O_3 / \Delta NO_x$) and total reactive nitrogen (Liu et al., 1987; Milford et al., 1994), satellite-retrieved proxies such as HCHO/NO_2 ratios (Jin et al., 2017, 2020), and

75   the sign of O_3 weekday-weekend difference as a natural experiment (Marr and Harley, 2002; De Foy et al., 2020). Additionally, metrics such as relative incremental reactivity and ozone isopleth diagrams can be derived using observation-constrained box models (Dodge, 1977; Cardelino and Chameides, 1995; Guo et al., 2023). As these methods rely on localized observations, they tend to neglect the effects of regional pollutant transport and mesoscale meteorology. The use of 3D chemical transport models addresses these limitations. In these models, ozone sensitivity can be evaluated through either brute-force emission perturbations

80   or more sophisticated sensitivity analysis techniques, such as *the adjoint method* used in this study. As an advanced receptor-oriented sensitivity analysis technique, the adjoint method can accurately compute the sensitivities of any user-defined air quality metric (*receptor*) with respect to emission changes at each grid cell, time step, and for each precursor species. The adjoint-based O_3-NO_x-VOC sensitivities are particularly policy-relevant, as they can directly pinpoint the most relevant sources for ozone receptors at urban, regional, and national scales (Pappin and Hakami, 2013; Wang et al., 2022, 2023; Hu et al., 2024). To our

85   knowledge, no prior studies have investigated meteorological impacts on adjoint-based O_3-NO_x-VOC sensitivities.

In this study, we assess how changes in meteorology alter O_3-NO_x-VOC sensitivity and optimal control strategies. We apply the adjoint method with a 3D chemical transport model to the San Joaquin Valley in central California, to quantify sensitivities of regional ozone formation to precursor emission changes across chemical species, space, and time. We analyze three distinct meteorological scenarios, each representing a physically coherent and historically observed episode: (1) typical summer

90   conditions (*baseline*), (2) a high-temperature case representing a heatwave (*high-T*), and (3) an episode with atmospherically stagnant conditions (*stagnation*). We evaluate not only changes in ozone responses, but also how meteorology shifts the type, location, and timing of the most influential precursor emissions.

Three emission inventory timeframes (2000, 2012 and 2022) are used in this study to capture a variety of chemical conditions. The year 2000 represents a more VOC-limited environment, whereas year 2022 reflects cleaner, NO_x-limited conditions

95   following major NO_x emission reductions. This study design allows us to investigate how meteorological effects vary across different chemical regimes, and how such influences may evolve on decadal timescales as emissions decline. Through this multi-scenario, multi-year framework, our findings offer insights into how ozone mitigation strategies should adapt in a warming climate.

2 Methodology

100   ### 2.1 Modeling Domain

The San Joaquin Valley (SJV) and adjacent air basins in central California (34.5-39°N, 118.5-123°W) are shown in Figure 1. The SJV is among the worst polluted regions in the United States, and is designated as an extreme ozone nonattainment area. The national standard for 8-hour ozone concentrations is 70 ppb, whereas SJV's design value has exceeded 85 ppb as of 2024, even after excluding wildfire impacts (San Joaquin Valley Air Pollution Control District, 2025). The poor air quality poses health

105   concerns for over four million SJV residents.

Land use in the SJV is characterized by widely extended agricultural activity, with major cities distributed along the main traffic corridor located on the east side of the valley (Highway 99, see Figure 1). The valley is bordered by the Sierra Neveda Mountains to the east and Coastal Mountain range to the west. On typical summer days, emissions of ozone precursors from upwind source regions including the San Francisco Bay area (SF Bay) and the Sacramento Valley (SV) are transported into the

110   SJV. Within the valley, the prevailing wind direction is generally from the northwest to southeast.
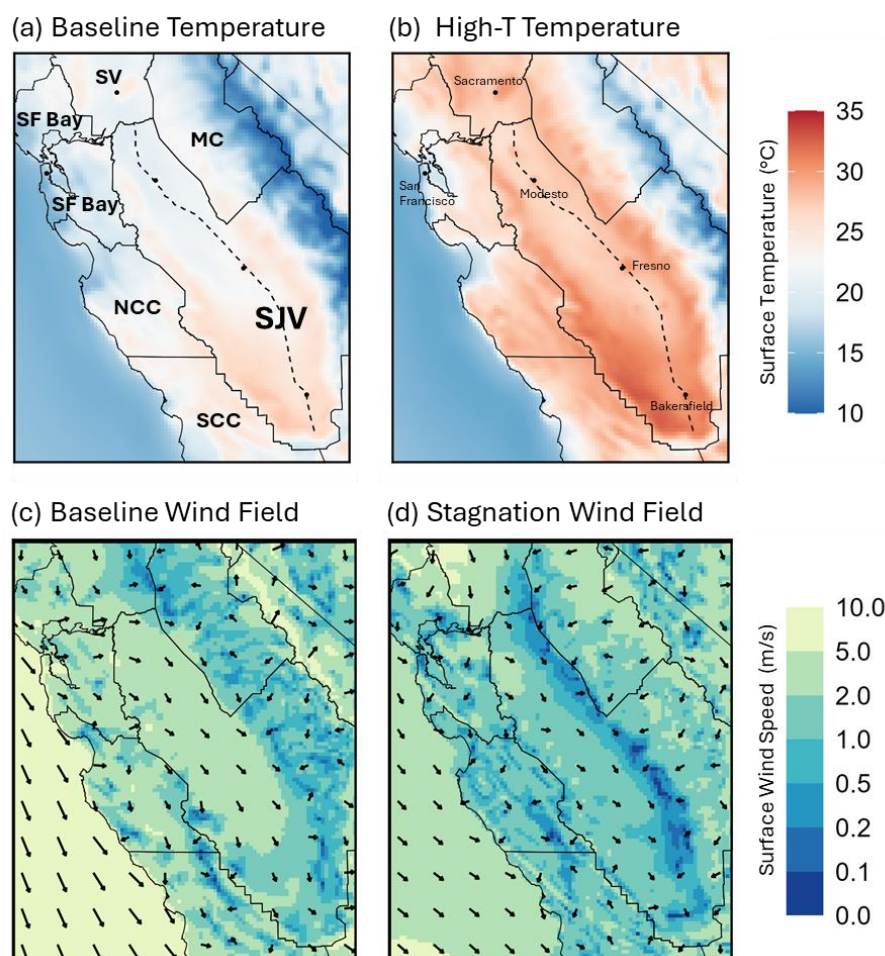
Figure 1. Daily average surface temperature (a-b) and wind fields (c-d). Air basins labeled in panel (a) include San Joaquin Valley (SJV), San Francisco Bay area (SF Bay), Sacramento Valley (SV), Mountain Counties (MC), North Central Coast (NCC) and South Central Coast (SCC). Major cities are shown in panel (b), with the dashed line representing Highway 99.

115

2.2 Meteorological Scenarios

Three meteorological scenarios are considered in this study: baseline, high-T, and stagnation. Each scenario encompasses a weeklong ozone episode (Table 1). These episodes are selected based on Jin et al. (2011), who applied K-means clustering to hourly meteorology and ozone fields across central California for an entire summer. Their analysis identified six statistically distinct meteorological regimes, each associated with unique ozone spatial distributions and pollution levels. From these, we

120 selected the three regimes that favor ozone formation and extracted typical meteorological conditions for weeklong timeframes within each regime. The three regimes differ primarily either in temperature (baseline vs. high-T), or in flow patterns (baseline vs. stagnation), with simultaneous changes in interconnected meteorological variables captured. This cluster-based approach offers a few advantages. First, it preserves the physical coherence of meteorological fields, in contrast to artificial perturbations

125   of individual variables. Second, these regimes are seen as recurring features across summers, so our scenario design has
       implications beyond one single year. Our findings can help anticipate how climate-induced changes in the frequency and
       intensity of such regimes will alter O_3-NO_x-VOC sensitivities and control effectiveness over time.

       Gridded meteorological fields at 4 km resolution are simulated for the baseline, high-T, and stagnation scenarios using their
       corresponding episodes (Table 1) in the fifth-generation Penn State/NCAR Mesoscale Meteorological Model (MM5; Grell et al.,

130   1994). These hourly fields – including wind, temperature, pressure, boundary layer dynamics, and radiation – are subsequently
       used as inputs for air quality modeling and sensitivity evaluation. Table 1 summarizes daily average surface temperatures and
       wind speeds, as well as daytime (10am–6pm) PBL heights under each scenario. Figure 1 contrasts surface temperature fields
       between baseline and high-T cases, and wind fields between baseline and stagnation. Diurnal evolutions of meteorological fields
       are shown in Supporting Figures S1–S3.

135   **Table 1**. Meteorological scenarios used in the study.

Scenario	Episode	Daily T (°C)*	Daily Wind (m/s)*	10am-6pm PBL (m)*
Baseline	11 – 17 August, 2000	24	2.3	600
High-T	27 July – 2 August, 2000	29	1.8	622
Stagnation	14 – 20 September, 2000	26	1.1	467

       * Values shown are averaged across the SJV air basin (excluding mountain grid cells)

       The *baseline* scenario features relatively ventilated conditions (daily mean wind speed ~2.3 m/s) and a moderate daily average
       temperature of ~24°C (Figure 1a). Strong westerly winds along with inflows from the north carry ozone precursors into the SJV
       and transport them southward along its axis (Figure 1c). The 10am-6pm planetary boundary layer (PBL) height is ~600 m,

140   indicative of moderate vertical mixing conditions.

       The *high-T* scenario is characterized by a +5°C temperature anomaly relative to baseline (Figure 1b). Its flow patterns and PBL
       heights resemble the baseline (Figures S1-S2), although wind speeds are ~20% slower. This meteorological regime typically
       corresponds to the presence of a persistent high-pressure ridge over the western U.S., which promotes subsidence, suppresses
       cloud cover, and results in consecutive days of elevated surface temperatures.

145   The *stagnation* scenario represents an atmospheric stagnation event. Its conditions satisfy commonly used stagnation criteria,
       including weak surface and mid-troposphere winds, and minimal precipitation (Wang and Angell, 1999). Compared to baseline,
       this scenario exhibits 53% and 22% reductions in average wind speeds and PBL heights, respectively (Table 1, Figure 1d).
       Although a modest (+2°C) temperature anomaly is part of this scenario (Figure S3), the primary driver of sensitivity changes in
       this case is attributed to stagnation rather than temperature effects. Jin et al. (2013) linked this meteorological regime with an

150   anticyclone system in the Northeastern Pacific, which heats up air over the ocean and in coastal areas and weakens the pressure
       gradient that drives onshore flow. The resulting stagnation limits pollutant inflow from upwind areas and inhibits pollutant
       outflow at the southern end of the valley, thereby increasing pollutant residence times.

2.3 Data and Model Setup

155   The Community Multiscale Air Quality Model (CMAQ) version 4.5 and its adjoint are used in this study with the same configuration (Byun and Schere, 2006; Hakami et al., 2007; Bastien et al., 2015, 2019). The CMAQ model simulates atmospheric chemistry and transport processes, while CMAQ Adjoint computes the sensitivities of a user-defined metric (*receptor*) with respect to emission changes. Here, the receptor is defined to be population-weighted 8-hour average (10am-6pm) concentration of odd oxygen ($O_x = O_3 + NO_2$) within the SJV.

160   The study domain (Figure 1) is gridded into 96×117 horizontal grid cells at 4-km resolution with 35 vertical layers. The piecewise parabolic method is used for advection, horizontal diffusion, and eddy vertical diffusion. Chemical reactions are represented using the SAPRC99 mechanism, which includes 72 species and 211 reactions (Carter, 2000). Hourly meteorological inputs for baseline, high-T, and stagnation scenarios are processed from MM5 model outputs (Grell et al., 1994). Time-resolved boundary conditions are derived from the Model for Ozone and Related chemical Tracers (MOZART-4; Emmons et al., 2010).

165   Biogenic emissions are driven by episode-specific meteorological conditions and estimated using BEIGIS (Scott and Benjamin, 2003). Anthropogenic emissions are provided by the California Air Resources Board for three different years (2000, 2012 and 2022) and are held constant across meteorology. Anthropogenic emissions show 45% and 41% reductions for NO_x and VOC during 2000-2012, and 42% and 13% reductions during 2012-2022 (Figures S4-S5).

170   **2.4 Adjoint-based Ozone Sensitivity Evaluation**

Nine sets of model simulations are performed for three meteorological scenarios (baseline, high-T, stagnation) and three emission scenarios (2000, 2012, 2022). Each scenario combination involves two model runs. First, a CMAQ run is used to evolve pollutant concentration fields by numerically solving a coupled set of partial differential equations of the form

$$\frac{\partial C_i}{\partial t} = -u \cdot \nabla C_i + \frac{1}{\rho} \nabla \cdot (\rho K_i \nabla C_i) + R_i(C) + E_i \qquad (1)$$

where C_i is the concentration of species i, u is the vector wind field, ρ is the air density, K_i is the diffusivity tensor, R_i is the net

175   formation rate by chemical reactions, and E_i represents emissions (Byun and Schere, 2006).

Second, a CMAQ adjoint run is performed, which uses data fields saved from the prior CMAQ run and numerically solves another set of partial differential equations in backward time order:

$$-\frac{\partial \lambda_i}{\partial t} = u \cdot \nabla \lambda_i + \nabla \cdot \left(\rho K_i \nabla \frac{\lambda_i}{\rho} \right) + F_i^T \lambda_i + \varphi_i \qquad (2)$$

where λ_i is called the adjoint variable, F_i^T is the ith row of the transposed Jacobian of the chemical reaction rates, and φ_i is the forcing term. The mathematical derivation of this adjoint model is detailed elsewhere (e.g., Sandu et al., 2005). Both the forcing

180   term (φ_i) and the adjoint variable (λ_i) depend on the choice of receptor. The receptor in this study is defined as the population-weighted 8-hour average O_x ($O_3 + NO_2$) concentration over the SJV. Solving the adjoint model yields $\lambda_i(x, y, z, t)$, which represents sensitivity of the receptor to concentration changes of species i at location (x, y, z) and time t.

We postprocess these λ_i outputs to calculate sensitivity of receptor (i.e., SJV population-weighted 8-hour O_x) with respect to proportional surface emission changes (E) of species i at location (x, y, z) and time t:

$$S_i(x, y, t) = E_i(x, y, t) \times \frac{\partial \, SJV \, Ox}{\partial E_i}\Bigg|_{(x,y,t)} \tag{3}$$

185 Notably, these sensitivity values, $S_i(x, y, t)$, are the primary focus of our analysis, representing first-order estimates of ozone contributions from specific source locations, emission periods, and precursor groups (hereafter "*contributions*" and "*sensitivities*" are used interchangeably).

To assess ozone formation regimes and source impacts, we aggregate sensitivity values by precursor group (e.g., NO_x, anthropogenic VOC, biogenic VOC), emission source region (e.g., local, non-local), and emission timing (e.g., same-day, prior-

190 day). We denote a chemical regime as "NO_x-limited" when the Ox sensitivity to NO_x exceeds that to anthropogenic VOC, and as "VOC-limited" otherwise. We then evaluate how these sensitivities and chemical regimes shift under varying meteorology, and how such meteorological influences differ in 2000, 2012, and 2022 chemical environments.

Model performance of both CMAQ and CMAQ adjoint has been evaluated in detail for this study domain, as described in Jin et al. (2010) and Wang et al. (2022). The standalone CMAQ model is evaluated using ambient observations of ozone and its

195 precursors collected during the Central California Ozone Study (Fujita et al., 2001). Stable model performance is found on both seasonal and episodic timescales, and our configuration options are optimized based on the diagnostic evaluations conducted in Jin et al. (2010). For the CMAQ adjoint model, its sensitivity outputs cannot be directly compared with observations and are instead evaluated against perturbation-based sensitivities. A total of 300 emission perturbations are implemented in CMAQ, each perturbing emissions of one specific species at an individual grid cell. High consistency is seen between adjoint and perturbation-

200 derived sensitivities, with a coefficient of determination at $R^2 = 0.96$ (Wang et al., 2022), confirming the validity of the adjoint framework for quantifying ozone sensitivity to precursor emissions in this domain.

3 Results and Discussion

Our research findings are presented in four parts. First, we summarize scenario-induced variations in the SJV ozone pollution

205 level and sensitivity magnitude, with a description of key sensitivity patterns for the baseline meteorology. The second and third sections examine in detail the effects of elevated temperature (high-T) and stagnation, respectively, through comparisons with baseline results. We discuss the underlying drivers and the consistency of meteorological influences over time. Finally, we identify key source locations to target that are effective across meteorological regimes, suggesting that climate-resilient air pollution mitigation strategies are both feasible and essential.

210

3.1 Variation Overview and Baseline Results

Table 2 summarizes SJV O_x levels across all scenario combinations, with O_x spatial distributions shown in Figure S6. Across years, the highest O_x values consistently occur under stagnant conditions (+7-10 ppb relative to baseline), followed by high-T (+4-6 ppb) and then baseline conditions. Long-term emission reductions demonstrate substantial effectiveness, as the O_x receptor

215 decreases by 11-15 ppb from 2000 to 2012, and by an additional 4-6 ppb from 2012 to 2022. Notably, in recent years, meteorology-induced variability has become comparable in magnitude to decadal-scale emission-driven changes. For example, under 2022 stagnant conditions, the SJV O_x burden (62.2 ppb) exceeds that of the 2012 baseline (57.3 ppb), highlighting the role of meteorology in modulating ozone pollution.

Table 2. SJV population-weighted 8-hour average O_x concentrations (in ppb) across scenarios.

	2000	**2012**	**2022**
Baseline	70.6	57.3	52.2
High-T	76.2	61.5	55.7
Stagnation	77.3	66.5	62.2

220

From a sensitivity perspective, the dominant precursor type and source locations vary greatly across scenarios. Figure 2 shows spatiotemporally aggregated sensitivity of O_x to anthropogenic VOC (AVOC) and NO_x. Over time, a clear shift in the ozone formation regime is seen, from VOC-limited in 2000 to NO_x-limited in 2022, as sensitivity to NO_x continuously rises and sensitivity to AVOC declines. This trend is driven by the more rapid reductions in NO_x compared to AVOC emissions over the

225 past two decades (Figure S4), and aligns with observational evidence from prior studies (Pusede and Cohen, 2012; De Foy et al., 2020).
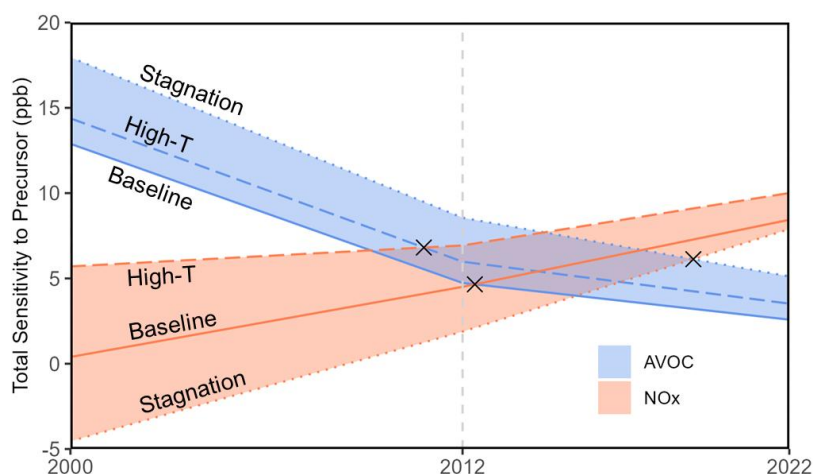
Figure 2. Sensitivities of SJV O_x to AVOC (blue) and NO_x (orange) emissions, aggregated over the simulation period and study domain. Color bands show meteorologically-induced variations. Cross marks indicate the points at which the chemical regime

230 switches (when NO_x contributions start to outweigh AVOC contributions).

Although the direction of this shift toward a NO_x-limited regime is consistent across meteorological scenarios, the timing of this regime switch (cross marks in Figure 2) can be accelerated or delayed depending on meteorology. Taking the 2012 case as an example, NO_x contribution has dominated under high-T conditions, but AVOC contribution is still 4.5 times NO_x contribution

235 under stagnation. This finding has important implications for other regions, especially those near the transition point, suggesting that episodic meteorological variability can substantially alter the chemical regime and is an essential consideration for designing robust mitigation strategies.

Overall, meteorological impacts on sensitivities are comparable in magnitude to those of decadal-scale emission changes. High-T conditions enhance sensitivity totals by 1.6-5.3 and 0.9-1.5 ppb, respectively, for NO_x and AVOC. Stagnation reduces NO_x
240   sensitivity by 0.5-4.9 ppb and amplifies AVOC sensitivity by 2.5-5.1 ppb. These shifts are in the same order as the sensitivity changes observed from 2000 to 2022 due to emission controls. In the following sections, high-T and stagnation results are compared against baseline to isolate meteorological influences. Key patterns of baseline sensitivities are summarized here as references for later comparisons.

Under baseline meteorology, anthropogenic contributions are from both local (SJV, 32-49%) and non-local sources (51-68%),
245   with the San Francisco Bay area and Sacramento Valley being the top non-local contributors (Figure S7). Biogenic contributions are relatively small in magnitude, accounting for 15-29% of total sensitivity, primarily from isoprene (81-85%) and monoterpene (11-14%) sources in coastal forests, the Sierra Nevada Mountains, and the northern SJV (Figure S8). Within the SJV, influential source locations – either positive or negative in sign depending on year – are concentrated along the urbanized Highway 99 corridor (see leftmost columns in Figure 4). The prevailing along-valley flow under baseline conditions facilitates pollutant
250   transport towards the southern end of the SJV, amplifying the influence of sources located along plume trajectories that intersect major cities (e.g., Fresno, Bakersfield; Figure S9). Peak sensitivities occur along the northern and central segments of Highway 99 and in cities nearby, where high emissions coincide with favorable transport pathways toward population centers.

A long-term shift in prevailing chemical regime is evident under baseline conditions, with the most influential source locations (northern and central segments of Highway 99) experiencing a change in sign from negative NO_x contributions in 2000 to
255   positive in 2022. The 2012 scenario marks a transitional case, as the majority (71%) of SJV grid cells show NO_x sensitivities that outweigh AVOC sensitivities, though the opposite remains true in urban and suburban areas (Figure S10). The cities of Fresno and Bakersfield appear to be among the last source areas to undergo the regime switch, as they continue to exhibit negative NO_x sensitivity through 2012.

260   **3.2 Temperature Impacts**

The comparison between baseline and high-T scenarios features a widespread increase in surface temperatures, with daily average values rising from 24 to 29 °C within the SJV (Table 1). Anthropogenic emissions are held constant for a given year despite the temperature increase, while biogenic VOC (BVOC) emissions are meteorology-driven and increased by ~17%. Across all years, the high-T scenario leads to increases of 4-6 ppb SJV O_x (Table 2). This is consistent with prior studies that note
265   a positive correlation between temperature and ozone pollution (Bloomer et al., 2009; Pusede et al., 2014; Coates et al., 2016).

From the sensitivity perspective, high-T amplifies SJV O_x sensitivities across years, for both NO_x and VOC, anthropogenic and biogenic, local and non-local sources. Biogenic contributions show a particularly strong relative increase, accounting for 15-29% of total sensitivity under baseline and 22-32% under high-T. For anthropogenic emissions, the spatial partitioning between local and non-local contributions remains similar between baseline and high-T scenarios, with local sources accounting for 31-32%,
270   40-45% and 47-49% of anthropogenic sensitivities in 2000, 2012, and 2022, respectively. In contrast, high-T effects on the ozone formation regime and the relative importance of AVOC versus NO_x control are more complex, varying with source location and emission scenario as discussed below.
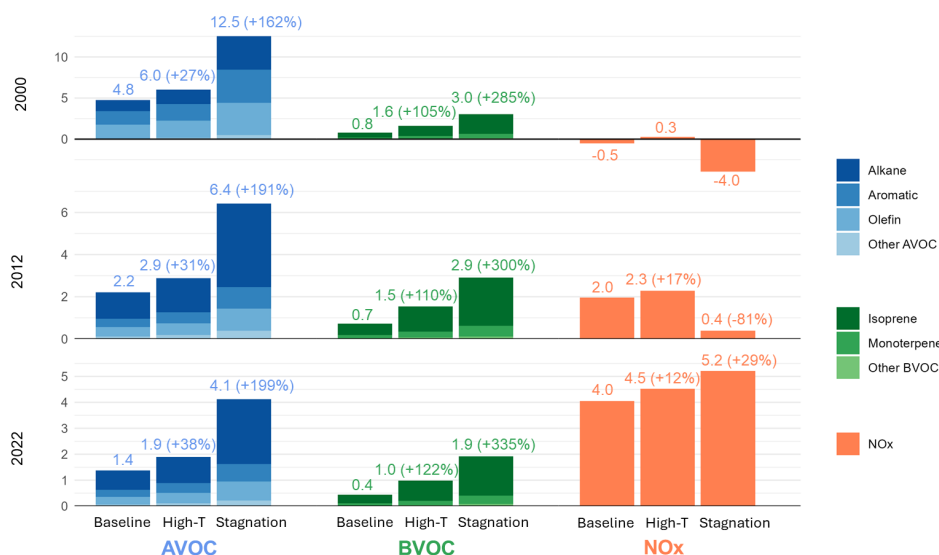
Figure 3. Sensitivities (ppb) of SJV O_x to AVOC (blue), BVOC (green) and NO_x (orange) emissions, grouped by species type and scenario. The values shown are summed over the entire SJV air basin. Percentages in parentheses indicate relative changes from baseline.

Across the SJV, the high-T case increases sensitivity by 0.3-0.8 ppb for NO_x, and by 0.5-1.2 ppb for AVOC across emission scenarios (Figure 3). These sensitivity increases are because high-T enhances the generation of HO_x radicals and accelerates temperature-dependent reactions to more efficiently form ozone. In 2000, when the region is characterized by high NO_x emissions and VOC-limited chemistry, elevated HO_x radicals raise the NO_x threshold for regime switch, therefore shifting the chemistry toward NO_x-limited conditions. Under the more NO_x-limited conditions of 2012 and 2022, high-T conditions moderately increase the relative importance of AVOC control, as AVOC contributions increase more substantially (+31-38%) than those for NO_x (+12-17%).

Contributions to overall VOC sensitivities by chemical species groupings are shown in Figure 3. AVOC contributions are primarily driven by alkanes, aromatics, and olefins, which together account for >90% of the totals. Under high-T conditions, sensitivities to these three groups increase by similar percentages (+22-40%), with no single group showing disproportionately larger temperature impacts. On the other hand, BVOC sensitivities are dominated by isoprene and monoterpene, both exhibiting larger relative increases compared to AVOC. Isoprene contributions within the SJV rise by 117-133%, while monoterpene contributions increase by 64-75%. Despite these increases, BVOC contributions remain smaller than AVOC under high-T conditions.
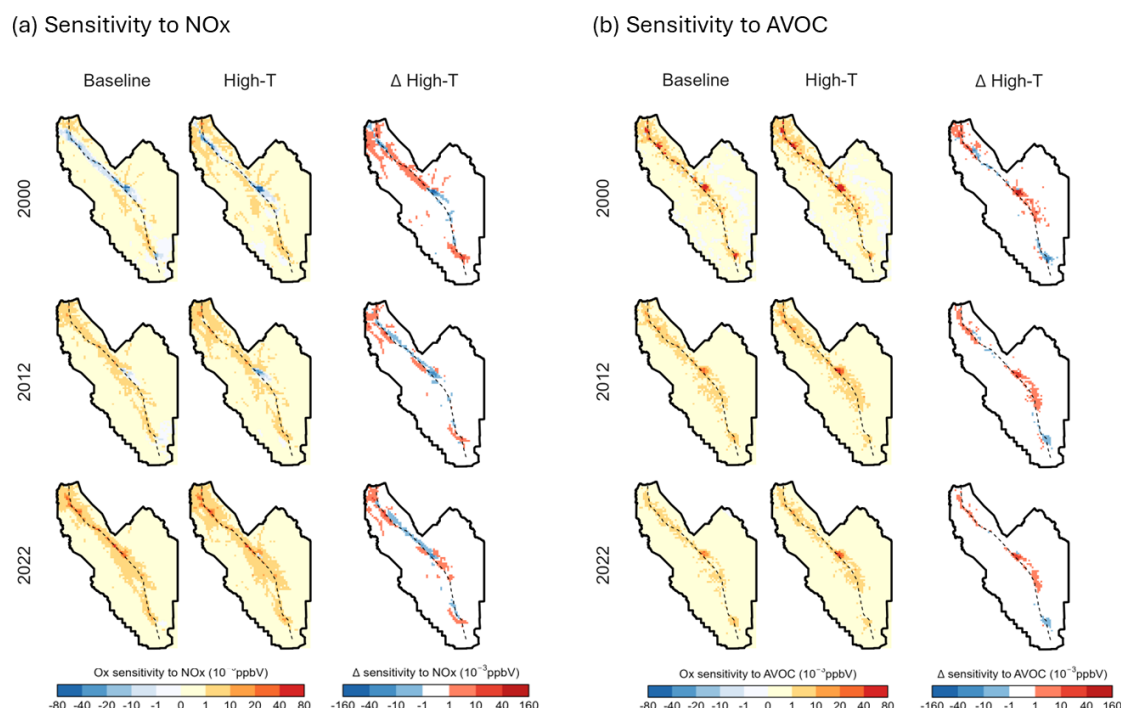
Figure 4. Sensitivities of the SJV O_x receptor to (a) NO_x and (b) AVOC emissions under baseline and high-T conditions for 2000, 2012, and 2022. Each panel shows sensitivities under baseline (left column), high-T (middle column), and the difference (high-T minus baseline, right column), with each row corresponding to a different emission inventory year. Higher values indicate larger contributions from the corresponding source locations to the SJV O_x receptor.

Figure 4 compares spatial distributions of NO_x and AVOC sensitivities within the SJV under baseline and high-T conditions. While sensitivity totals for both precursors increase (Figure 3), their enhancements typically occur at different locations (Figure 4). At the grid cell level, temperature-induced changes in NO_x and AVOC sensitivities tend to be opposite in sign, with consistently negative correlations across years (Figure S11). In the southern end of the valley, NO_x sensitivities increase and AVOC sensitivities decline with temperature, while the opposite trend is observed in the middle portion of the SJV valley near Fresno. The northern SJV exhibits a mix of both behaviors.

Overall, the optimal source locations for emission control are not substantially shifted by temperature, with the only exception being NO_x in the earliest (2000) emission inventory. When ranking SJV grid cells by their individual contributions to the O_x receptor, the correlations between high-T and baseline rankings are R = 0.75-0.97 for NO_x, and R = 0.97-0.98 for AVOC (see Figure S12). The lowest correlation coefficient (0.75 for NO_x as of 2000) reflects a shift in chemical regime at certain influential source locations (e.g., Bakersfield and the northern SJV), where high-T drives the chemistry toward a more NO_x-limited state and reverses the sign of NO_x contributions, thus elevating these areas from low- to top-priority targets for emission control.

3.3 Stagnation Impacts

The stagnation scenario is characterized by reduced boundary layer heights, weak surface winds, and diminished coastal inflows. Biogenic emissions are similar to baseline (difference < 5%), and anthropogenic emissions remain constant. Under stagnant conditions, SJV O_x increases by 7-10 ppb relative to baseline (Table 2). Unlike high-T impacts, stagnation markedly alters both the magnitude and spatial distributions of sensitivity. As illustrated in Figure 5, it significantly shifts the relative importance of NO_x versus VOC, anthropogenic versus biogenic, local versus non-local, and prior-day versus same-day sources. While this visualization only shows results for 2022, the patterns discussed below generally hold true across emission scenarios.
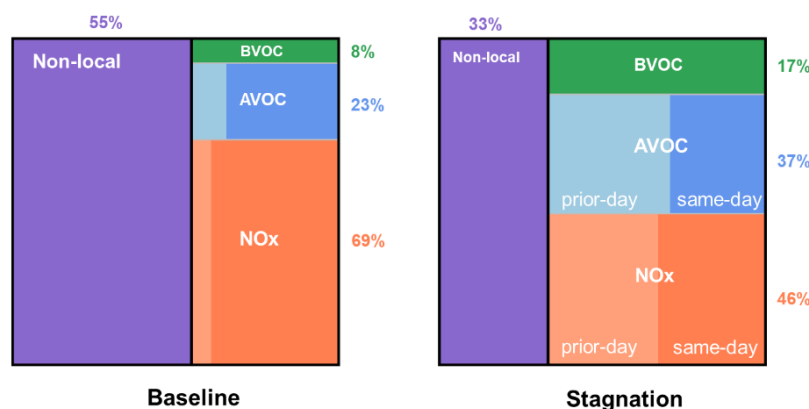
Figure 5. Source contributions to SJV O_x under baseline (left) and stagnant (right) conditions for 2022. Each panel shows the relative contributions from non-local sources (purple), as well as local BVOC (green), AVOC (blue) and NO_x (orange) sources within the SJV. Local AVOC and NO_x sensitivities are further attributed to same-day (darker shading) versus prior-day (lighter shading) emissions.

Stagnation significantly amplifies the relative importance of local emission sources. Under baseline conditions, SJV sources (anthropogenic and biogenic combined) account for 29-45% of total sensitivity, but this percentage rises to 56-67% under stagnant conditions. Meanwhile, the influence of San Francisco Bay area sources substantially declines from 32-41% to 4-7% under stagnation, as there is less inflow to the SJV and therefore reduced Bay area influence on ozone formation (Figure 1d). The other major non-local source area – Sacramento Valley (SV) – shows relatively stable contributions across meteorology, accounting for 13-17% of total sensitivity under baseline and 18-19% under stagnation.

Within the SJV, substantial sensitivity increases are observed for prior-day emissions, due to prolonged residence times and enhanced carryover effects. Under baseline meteorology, O_x sensitivity to local sources is predominantly attributed to same-day emissions (66-82%), followed by emissions from one day prior (15-27%). For stagnant conditions, however, prior-day emissions from one day (37-44%) and two days (17-28%) prior outweigh same-day source contributions to O_x formation (28-36%), highlighting the need for anticipatory emission planning and multi-day control strategies to mitigate stagnation-induced ozone episodes.

Most notably, stagnation consistently drives the ozone chemistry to become more VOC-limited. Figure 2 shows that stagnation increases AVOC sensitivity by 2.5-5.1 ppb and decreases NO_x sensitivity by 0.5-4.9 ppb on a domain-wide level. Figure 3 further

shows enhancements in AVOC and BVOC sensitivities by +160-200% and +285-335% within the SJV, whereas NO_x sensitivity either decreases (for 2000 and 2012) or increases modestly (for 2022). Major AVOC species alkanes, aromatics, and olefins see

340   sensitivity increase by +201-233%, +144-160%, +129-141%, respectively, and major BVOC species isoprene and monoterpene see sensitivity increase by +313-351% and +188-261%. Overall, the relative importance of VOC control substantially rises under stagnation and is comparable to NO_x even in 2022 (Figure 5), which is a clearly NO_x-limited case under baseline meteorology.

Figure 6 contrasts spatial sensitivity patterns between baseline and stagnation scenarios. For both precursor types, there is a noticeable expansion of influential source areas under stagnation, especially near the center of the SJV. Under baseline

345   conditions, impactful sources are mainly aligned with along-valley flow trajectories that intersect major cities. During a stagnation event, however, lower boundary layers and weaker winds limit outflows at the southern end, strengthening return flows and eddy recirculation within the valley. A larger spatial range of sources can now interact with urban plumes and contribute to O_x formation. This transport-driven effect helps explain the modest increase in local NO_x contributions in 2022 (Figure 3), despite an overall shift toward VOC-limited chemistry. Chemistry-driven reductions in NO_x sensitivities dominate in

350   the northern and southern SJV, while transport-driven enhancements are more apparent in the middle portion of the SJV. Together, the net change in SJV NO_x contribution is negative in 2000 and 2012, but becomes slightly positive in 2022 when transport-driven effects outweigh regime shift effects.
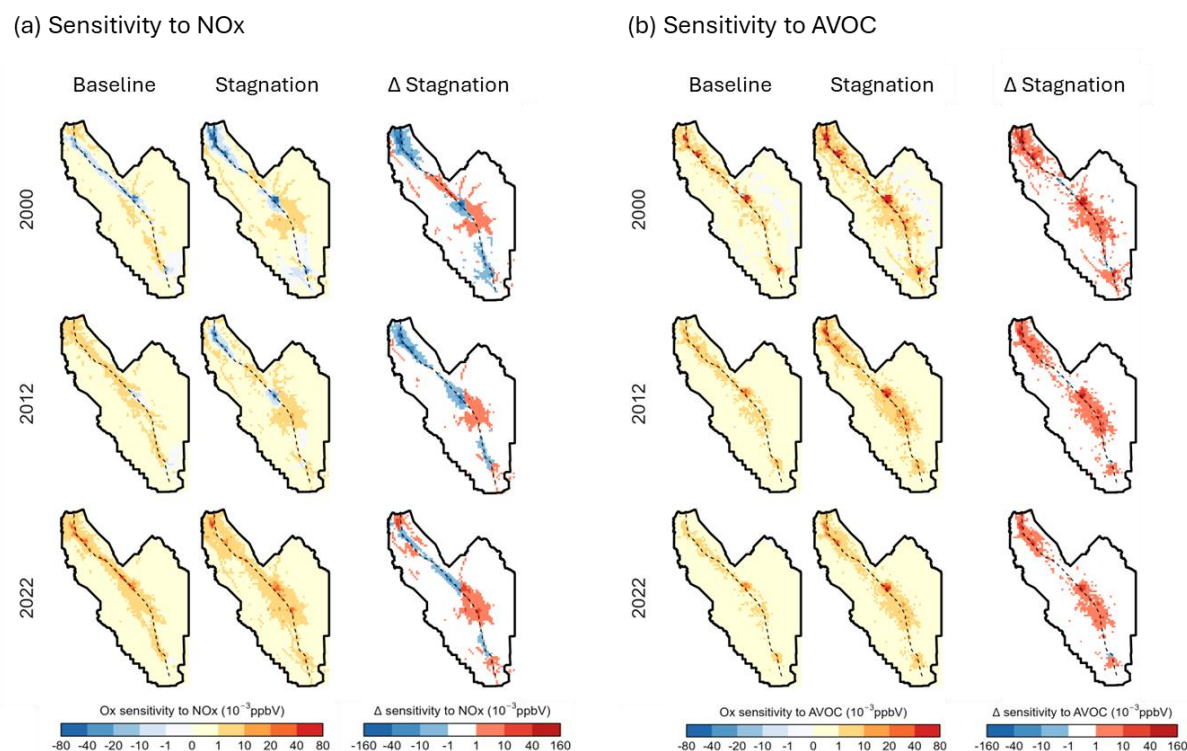
Figure 6. Sensitivities of SJV O_x to (a) NO_x and (b) AVOC emissions under baseline and stagnant conditions. Each panel shows

355   sensitivities under baseline (left column), stagnation (middle column), and the difference (stagnation minus baseline, right column), with each row corresponding to different emission inventory scenarios. Higher values indicate larger contributions from the corresponding source locations to SJV O_x.

Overall, stagnation can shift optimal source locations, and especially so for NO_x control in VOC-limited (2000) or transitional

360 (2012) environments. The stagnation-induced regime shift toward VOC limitation triggers a sign switch in sensitivity within some major NO_x source regions, and the transport-driven effects lead to emergence of new sensitivity hotspots in the valley center. We find poor correlations between stagnation and baseline rankings of SJV grid cells by their individual NO_x contributions, with R = 0.49, 0.57, and 0.94 in 2000, 2012, and 2022 (Figure S13). These correlation values highlight that stagnation can substantially alter optimal control targets – especially for NO_x – by reshaping both chemical regimes and pollutant

365 transport patterns.

3.4 Climate-Resilient Ozone Mitigation

As demonstrated in prior sections, changes in prevailing meteorological conditions – specifically high temperatures and stagnation – can substantially alter ozone precursor sensitivities, chemical regimes, and the most effective source locations for

370 emission control. These changes highlight that mitigation strategies designed under average conditions may fall short under extreme weather events, which are expected to become more frequent with climate change. To support robust control strategy design, Figure 7 identifies SJV grid cells that consistently rank among the top 10% of contributors to O_x formation under all three meteorological scenarios. These maps serve as a screening tool for pinpointing "climate-resilient" source areas where emission reductions consistently yield strong ozone benefits, regardless of weather conditions.

375
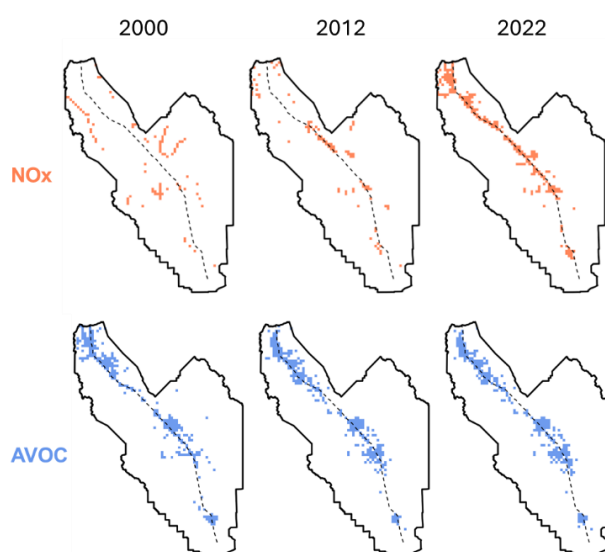
Figure 7. Optimal SJV emission source locations to target for control where sensitivities to NO_x (top row) and AVOC (bottom row) emissions consistently rank in the top 10% across meteorological scenarios in 2000, 2012, and 2022. The dashed line represents Highway 99.

Figure 7 reveals spatial differences in the optimal strategies that target NO_x versus AVOC emissions. For NO_x, relatively few source locations are impactful across meteorology in early years (2000 and 2012), with only ~2.5% of SJV grid cells consistently ranking among the top 10% contributors. This reflects the high variability of NO_x control effectiveness to meteorological changes. The overlap increases for 2022, with 6.2% of SJV grid cells consistently identified as top 10% contributors, indicating that the spatial stability of optimal locations for NO_x control improves as the chemical environment transitions toward NO_x limitation. In contrast, the optimal locations for AVOC control are quite stable with respect to meteorological variations. As shown in Figure 7, climate-robust AVOC target locations for emission control account for 7.3-7.6% of grids cells in the SJV across emission scenarios and are consistently distributed along Highway 99.

Over time, we find a growing subset of sources that remain influential across meteorological scenarios, accompanied by increasing spatial convergence in source targets between NO_x and VOC. These trends create opportunities for the SJV to design co-control programs that are both spatially targeted and robust to weather variability. The implications extend beyond the SJV to other regions in VOC-limited or transitional regimes. As anthropogenic emissions decline and ozone chemistry shifts toward NO_x limitation, there is reduced influence of meteorology variability on optimal strategy design. Thus, emission reductions not only bring direct benefits for lowering pollution levels, but also enable the development of climate-resilient control programs to maintain healthy air quality under meteorology extremes.

4 Conclusions

This study employs the CMAQ adjoint model to explore how high temperature and stagnant meteorology affect ozone sensitivity to precursor emissions in California's San Joaquin Valley (SJV) under three distinct emission scenarios (2000, 2012, and 2022). While prior work has emphasized the role of meteorology in modulating ozone levels, our results highlight its underappreciated influence on chemical sensitivity, source-receptor relationships, and ultimately the design of optimal ozone mitigation strategies. We find that meteorology-driven sensitivity changes can be comparable in magnitude to those from decadal emission reductions.

High-temperature conditions (+5 °C) broadly enhance ozone sensitivity across precursor types and source regions. Sensitivity to biogenic VOC is more than doubled, despite only ~17% increases in its emissions. In a VOC-limited environment (e.g., the 2000 emission), high-T shifts the ozone regime toward NO_x limitation, altering the effectiveness of NO_x control and changing optimal source locations to target. In contrast, under NO_x-limited conditions (e.g., the 2022 emission), optimal source targets remain more stable and the relative importance of VOC control increases.

Stagnation, on the other hand, consistently shifts ozone chemistry toward VOC limitation. VOC contributions can be up to 4 times higher than baseline, while sensitivity to NO_x generally declines or only modestly rises. Impacts of local prior-day sources are substantially amplified under stagnation, as lower boundary layer heights and weaker winds enhance pollutant recirculation and carryover effects. We also find substantial spatial shifts in optimal source targets, though stability improves over time as the region transitions into a NO_x-limited regime.

Taking these variations into account, we identify climate-resilient source targets for effective ozone mitigation regardless of meteorology variability. On decadal timescales, we find a wider range of "climate-resilient" targets and a spatial convergence between NO_x and VOC sources over time. As the chemical environment continues to evolve, our findings suggest that

415   incorporating meteorological extremes into mitigation planning becomes both necessary and feasible to sustain long-term ozone
       air quality goals.

Competing interests

Yuan Wang is a member of the editorial board of Atmospheric Chemistry and Physics.

Acknowledgements

420   This research was supported by the California Energy Commission under contract EPC-17-028. Model simulations were
       conducted on the Lawrencium high performance computing cluster at Lawrence Berkeley National Laboratory. We thank Jeremy
       Avise at the California Air Resources Board for providing the gridded emission inventory for year 2012, and Wei Zhou, Huy
       Phan, and Tin Ho for their assistance in emission and meteorological input data processing and model testing.

Author Contributions

425   YhW: conceptualization, methodology, formal analysis, visualization, writing – original draft. LB: methodology, formal analysis,
       writing – review and editing; YW: formal analysis, visualization, writing – review and editing. LJ: conceptualization,
       methodology, formal analysis, visualization, writing – review and editing, funding acquisition. RH: conceptualization,
       methodology, formal analysis, visualization, writing – review and editing, funding acquisition.

Code and Data Availability

430   CMAQ adjoint v4.5 model is available at https://people.cs.vt.edu/~asandu/Software/CMAQ_ADJ/CMAQ_ADJ.html. Key inputs
       and output data are provided at https://github.com/yhanw0719/paper_met_o3_adj, and more detailed data are available upon
       request.

References

Baertsch-Ritter, N., Keller, J., Dommen, J., and Prevot, A. S. H. (2004). Effects of various meteorological conditions and spatial
435   emissionresolutions on the ozone concentration and ROG/NO$_x$ limitationin the Milan area (I). *Atmospheric Chemistry
           and Physics*, *4*(2), 423–438. https://doi.org/10.5194/acp-4-423-2004

Bastien, L. A. J., Brown, N. J., and Harley, R. A. (2019). Contributions to local- and regional-scale formaldehyde concentrations.
           Atmospheric Chemistry and Physics, *19*(13), 8363–8381. https://doi.org/10.5194/acp-19-8363-2019

Bastien, L. A. J., McDonald, B. C., Brown, N. J., and Harley, R. A. (2015). High-Resolution Mapping of Sources Contributing to
440   Urban Air Pollution Using Adjoint Sensitivity Analysis: Benzene and Diesel Black Carbon. *Environmental Science &
           Technology*, *49*(12), 7276–7284. https://doi.org/10.1021/acs.est.5b00686

Biswas, J., and Rao, S. T. (2001). Uncertainties in Episodic Ozone Modeling Stemming from Uncertainties in the Meteorological
           Fields. *Journal of Applied Meteorology*, *40*(2), 117–136. https://doi.org/10.1175/1520-
           0450(2001)040<0117:UIEOMS>2.0.CO;2

445   Bloomer, B. J., Stehr, J. W., Piety, C. A., Salawitch, R. J., and Dickerson, R. R. (2009). Observed relationships of ozone air
     pollution with temperature and emissions. *Geophysical Research Letters*, *36*(9), 2009GL037308.
     https://doi.org/10.1029/2009GL037308

     Byun, D., and Schere, K. L. (2006). Review of the Governing Equations, Computational Algorithms, and Other Components of
     the Models-3 Community Multiscale Air Quality (CMAQ) Modeling System. *Applied Mechanics Reviews*, *59*(2), 51–
450   77. https://doi.org/10.1115/1.2128636

     Cardelino, C. A., and Chameides, W. L. (1995). An Observation-Based Model for Analyzing Ozone Precursor Relationships in
     the Urban Atmosphere. *Journal of the Air & Waste Management Association*, *45*(3), 161–180.
     https://doi.org/10.1080/10473289.1995.10467356

     Carter, W. P. (2000). Documentation of the SAPRC-99 chemical mechanism for VOC reactivity assessment. *Contract*, *92*(329),
455   95–308.

     Coates, J., Mar, K. A., Ojha, N., and Butler, T. M. (2016). The influence of temperature on ozone production under varying NO_x
     conditions – a modelling study. *Atmospheric Chemistry and Physics*, *16*(18), 11601–11615. https://doi.org/10.5194/acp-
     16-11601-2016

     De Foy, B., Brune, W. H., and Schauer, J. J. (2020). Changes in ozone photochemical regime in Fresno, California from 1994 to
460   2018 deduced from changes in the weekend effect. *Environmental Pollution*, *263*, 114380.
     https://doi.org/10.1016/j.envpol.2020.114380

     Dodge, M. (1977). Combined use of modeling techniques and smog chamber data to derive ozone-precursor relationships.
     International Conference on Photochemical Oxidant Pollution and Its Control: Proceedings, *2*, 881–889.

     Emmons, L. K., Walters, S., Hess, P. G., Lamarque, J.-F., Pfister, G. G., Fillmore, D., Granier, C., Guenther, A., Kinnison, D.,
465   Laepple, T., Orlando, J., Tie, X., Tyndall, G., Wiedinmyer, C., Baughcum, S. L., and Kloster, S. (2010). Description and
     evaluation of the Model for Ozone and Related chemical Tracers, version 4 (MOZART-4). *Geoscientific Model*
     Development, *3*(1), 43–67. https://doi.org/10.5194/gmd-3-43-2010

     Fujita, E., D. Campbell, R. Keisler, J. Brown, S. Tanrikulu, and A. J. Ranzieri (2001), Central California Ozone Study (CCOS) -
     Final report, volume III: Summary of field operations, technical report, California Air Resources Board, Sacramento.

470   Gao, Y., Fu, J. S., Drake, J. B., Lamarque, J.-F., and Liu, Y. (2013). The impact of emission and climate change on ozone in the
     United States under representative concentration pathways (RCPs). *Atmospheric Chemistry and Physics*, *13*(18), 9607–
     9621. https://doi.org/10.5194/acp-13-9607-2013

     Grell, G. A., Dudhia, J., Stauffer, D. R., and others. (1994). *A description of the fifth-generation Penn State/NCAR Mesoscale*
     Model (MM5).

475   Guo, J., Zhang, X., Gao, Y., Wang, Z., Zhang, M., Xue, W., Herrmann, H., Brasseur, G. P., Wang, T., and Wang, Z. (2023).
     Evolution of Ozone Pollution in China: What Track Will It Follow? *Environmental Science & Technology*, *57*(1), 109–
     117. https://doi.org/10.1021/acs.est.2c08205

     Hakami, A., Henze, D. K., Seinfeld, J. H., Singh, K., Sandu, A., Kim, S., Byun, and Li, Q. (2007). The Adjoint of CMAQ.
     Environmental Science & Technology, *41*(22), 7807–7817. https://doi.org/10.1021/es070944p

480   Horton, D. E., Skinner, C. B., Singh, D., and Diffenbaugh, N. S. (2014). Occurrence and persistence of future atmospheric
     stagnation events. *Nature Climate Change*, *4*(8), 698–703. https://doi.org/10.1038/nclimate2272

     Hou, P., and Wu, S. (2016). Long-term Changes in Extreme Air Pollution Meteorology and the Implications for Air Quality.
     Scientific Reports, *6*(1), 23792. https://doi.org/10.1038/srep23792

Hu, W., Zhao, Y., Lu, N., Wang, X., Zheng, B., Henze, D. K., Zhang, L., Fu, T.-M., and Zhai, S. (2024). Changing Responses of
    485   PM$_{2.5}$ and Ozone to Source Emissions in the Yangtze River Delta Using the Adjoint Model. *Environmental Science &*
            Technology, *58*(1), 628–638. https://doi.org/10.1021/acs.est.3c05049

Huang, M., Feng, Z., and Liao, T. (2025). Shift of surface O3-NOx-VOC sensitivity with temperature in the Guangdong-Hong
            Kong-Macao Greater Bay Area, South China. *Environmental Pollution*, *372*, 125974.
            https://doi.org/10.1016/j.envpol.2025.125974

    490 Jerrett, M., Burnett, R. T., Pope, C. A., Ito, K., Thurston, G., Krewski, D., Shi, Y., Calle, E., and Thun, M. (2009). Long-Term
            Ozone Exposure and Mortality. *New England Journal of Medicine*, *360*(11), 1085–1095.
            https://doi.org/10.1056/NEJMoa0803894

Jin, L., Brown, N. J., Harley, R. A., Bao, J., Michelson, S. A., and Wilczak, J. M. (2010). Seasonal versus episodic performance
            evaluation for an Eulerian photochemical air quality model. *Journal of Geophysical Research: Atmospheres*, *115*(D9),
    495   2009JD012680. https://doi.org/10.1029/2009JD012680

Jin, L., Harley, R. A., and Brown, N. J. (2011). Ozone pollution regimes modeled for a summer season in California's San
            Joaquin Valley: A cluster analysis. *Atmospheric Environment*, *45*(27), 4707–4718.
            https://doi.org/10.1016/j.atmosenv.2011.04.064

Jin, L., Loisy, A., and Brown, N. J. (2013). Role of meteorological processes in ozone responses to emission controls in
    500   California's San Joaquin Valley. *Journal of Geophysical Research: Atmospheres*, *118*(14), 8010–8022.
            https://doi.org/10.1002/jgrd.50559

Jin, L., Tonse, S., Cohan, D. S., Mao, X., Harley, R. A., and Brown, N. J. (2008). Sensitivity Analysis of Ozone Formation and
            Transport for a Central California Air Pollution Episode. *Environmental Science & Technology*, *42*(10), 3683–3689.
            https://doi.org/10.1021/es072069d

    505 Jin, X., Fiore, A., Boersma, K. F., Smedt, I. D., and Valin, L. (2020). Inferring Changes in Summertime Surface Ozone–NO$_x$ –
            VOC Chemistry over U.S. Urban Areas from Two Decades of Satellite and Ground-Based Observations. *Environmental*
            Science & Technology, *54*(11), 6518–6529. https://doi.org/10.1021/acs.est.9b07785

Jin, X., Fiore, A. M., Murray, L. T., Valin, L. C., Lamsal, L. N., Duncan, B., Folkert Boersma, K., De Smedt, I., Abad, G. G.,
            Chance, K., and Tonnesen, G. S. (2017). Evaluating a Space-Based Indicator of Surface Ozone-NO$_x$ -VOC Sensitivity
    510   Over Midlatitude Source Regions and Application to Decadal Trends. *Journal of Geophysical Research: Atmospheres*,
            122(19). https://doi.org/10.1002/2017JD026720

Kleinman, L. I. (2005). The dependence of tropospheric ozone production rate on ozone precursors. *Atmospheric Environment*,
            39(3), 575–586. https://doi.org/10.1016/j.atmosenv.2004.08.047

Krupa, S., McGrath, M. T., Andersen, C. P., Booker, F. L., Burkey, K. O., Chappelka, A. H., Chevone, B. I., Pell, E. J., and
    515   Zilinskas, B. A. (2001). Ambient Ozone and Plant Health. *Plant Disease*, *85*(1), 4–12.
            https://doi.org/10.1094/PDIS.2001.85.1.4

Liu, S. C., Trainer, M., Fehsenfeld, F. C., Parrish, D. D., Williams, E. J., Fahey, D. W., Hübler, G., and Murphy, P. C. (1987).
            Ozone production in the rural troposphere and the implications for regional and global ozone distributions. *Journal of*
            Geophysical Research: Atmospheres, *92*(D4), 4191–4207. https://doi.org/10.1029/JD092iD04p04191

    520 Marr, L. C., and Harley, R. A. (2002). Spectral analysis of weekday–weekend differences in ambient ozone, nitrogen oxide, and
            non-methane hydrocarbon time series in California. *Atmospheric Environment*, *36*(14), 2327–2335.
            https://doi.org/10.1016/S1352-2310(02)00188-7

Meehl, G. A., and Tebaldi, C. (2004). More Intense, More Frequent, and Longer Lasting Heat Waves in the 21st Century. *Science*, *305*(5686), 994–997. https://doi.org/10.1126/science.1098704

Milford, J. B., Gao, D., Sillman, S., Blossey, P., and Russell, A. G. (1994). Total reactive nitrogen (NO_y) as an indicator of the sensitivity of ozone to reductions in hydrocarbon and NO_x emissions. *Journal of Geophysical Research: Atmospheres*, *99*(D2), 3533–3542. https://doi.org/10.1029/93JD03224

Nussbaumer, C. M., and Cohen, R. C. (2020). The Role of Temperature and NO_x in Ozone Trends in the Los Angeles Basin. *Environmental Science & Technology*, *54*(24), 15652–15659. https://doi.org/10.1021/acs.est.0c04910

Pappin, A. J., and Hakami, A. (2013). Attainment vs Exposure: Ozone Metric Responses to Source-Specific NO_x Controls Using Adjoint Sensitivity Analysis. *Environmental Science & Technology*, *47*(23), 13519–13527. https://doi.org/10.1021/es4024145

Pfannerstill, E. Y., Arata, C., Zhu, Q., Schulze, B. C., Ward, R., Woods, R., Harkins, C., Schwantes, R. H., Seinfeld, J. H., Bucholtz, A., Cohen, R. C., and Goldstein, A. H. (2024). Temperature-dependent emissions dominate aerosol and ozone formation in Los Angeles. *Science*, *384*(6702), 1324–1329. https://doi.org/10.1126/science.adg8204

Pusede, S. E., and Cohen, R. C. (2012). On the observed response of ozone to NO_x and VOC reactivity reductions in San Joaquin Valley California 1995–present. *Atmospheric Chemistry and Physics*, *12*(18), 8323–8339. https://doi.org/10.5194/acp-12-8323-2012

Pusede, S. E., Gentner, D. R., Wooldridge, P. J., Browne, E. C., Rollins, A. W., Min, K.-E., Russell, A. R., Thomas, J., Zhang, L., Brune, W. H., Henry, S. B., DiGangi, J. P., Keutsch, F. N., Harrold, S. A., Thornton, J. A., Beaver, M. R., St. Clair, J. M., Wennberg, P. O., Sanders, J., … Cohen, R. C. (2014). On the temperature dependence of organic reactivity, nitrogen oxides, ozone production, and the impact of emission controls in San Joaquin Valley, California. *Atmospheric Chemistry and Physics*, *14*(7), 3373–3395. https://doi.org/10.5194/acp-14-3373-2014

Pusede, S. E., Steiner, A. L., and Cohen, R. C. (2015). Temperature and Recent Trends in the Chemistry of Continental Surface Ozone. *Chemical Reviews*, *115*(10), 3898–3918. https://doi.org/10.1021/cr5006815

San Joaquin Valley Air Pollution Control District. (2025). *2024 Annual Report to the Community*. https://www.valleyair.org/media/5h3bg1n4/annualreport2024-english.pdf

Sandu, A., Daescu, D. N., Carmichael, G. R., and Chai, T. (2005). Adjoint sensitivity analysis of regional air quality models. *Journal of Computational Physics*, *204*(1), 222–252.

Schnell, J. L., and Prather, M. J. (2017). Co-occurrence of extremes in surface ozone, particulate matter, and temperature over eastern North America. *Proceedings of the National Academy of Sciences*, *114*(11), 2854–2859. https://doi.org/10.1073/pnas.1614453114

Scott, K. I., and Benjamin, M. T. (2003). Development of a biogenic volatile organic compounds emission inventory for the SCOS97-NARSTO domain. *Atmospheric Environment*, *37*, 39–49.

Shen, L., Mickley, L. J., and Gilleland, E. (2016). Impact of increasing heat waves on U.S. ozone episodes in the 2050s: Results from a multimodel analysis using extreme value theory. *Geophysical Research Letters*, *43*(8), 4017–4025. https://doi.org/10.1002/2016GL068432

Steiner, A. L., Davis, A. J., Sillman, S., Owen, R. C., Michalak, A. M., and Fiore, A. M. (2010). Observed suppression of ozone formation at extremely high temperatures due to chemical and biophysical feedbacks. *Proceedings of the National Academy of Sciences*, *107*(46), 19685–19690. https://doi.org/10.1073/pnas.1008336107

Wang, J., and Angell, J. (1999). *Air Stagnation Climatology for the United States (1948-1998)*. NOAA/Air Resource Laboratory ATLAS.

Wang, Y., Bastien, L., Jin, L., and Harley, R. A. (2022). Responses of Photochemical Air Pollution in California's San Joaquin Valley to Spatially and Temporally Resolved Changes in Precursor Emissions. *Environmental Science & Technology*, *56*(11), 7074–7082. https://doi.org/10.1021/acs.est.1c07011

Wang, Y., Bastien, L., Jin, L., and Harley, R. A. (2023). Location-Specific Control of Precursor Emissions to Mitigate Photochemical Air Pollution. *Environmental Science & Technology*, *57*(26), 9693–9701. https://doi.org/10.1021/acs.est.3c01934

Yang, L., Yuan, Z., Luo, H., Wang, Y., Xu, Y., Duan, Y., and Fu, Q. (2021). Identification of long-term evolution of ozone sensitivity to precursors based on two-dimensional mutual verification. *Science of The Total Environment*, *760*, 143401. https://doi.org/10.1016/j.scitotenv.2020.143401

Zhang, J., Gao, Y., Luo, K., Leung, L. R., Zhang, Y., Wang, K., and Fan, J. (2018). Impacts of compound extreme weather events on ozone in the present and future. *Atmospheric Chemistry and Physics*, *18*(13), 9861–9877. https://doi.org/10.5194/acp-18-9861-2018